1521-0103/377/1/169–180$35.00
THE JOURNAL OF PHARMACOLOGY AND EXPERIMENTAL THERAPEUTICS

https://doi.org/10.1124/jpet.120.000457
J Pharmacol Exp Ther 377:169–180, April 2021

Organic Anion–Transporting Polypeptide 1B1/1B3–Mediated Hepatic Uptake Determines the Pharmacokinetics of Large Lipophilic Acids: In Vitro–In Vivo Evaluation in Cynomolgus Monkey[S]

Heather Eng, Yi-an Bi, Mark A. West, Sangwoo Ryu, Emi Yamaguchi, Rachel E. Kosa, David A. Tess, David A. Griffith, John Litchfield, Amit S. Kalgutkar, and Manthena V. S. Varma

ADME Sciences, Medicine Design, Worldwide Research and Development, Pfizer Inc., Groton, Connecticut (H.E., Y.B., M.A.W., S.R., E.Y., R.E.K., M.V.S.V.), and PDM (D.A.T., J.L., A.S.K.) and Medicinal Chemistry, Medicine Design, Worldwide Research and Development (D.A.G.), Pfizer Inc., Cambridge, Massachusetts

Received December 7, 2020; accepted January 25, 2021

ABSTRACT

It is generally presumed that uptake transport mechanisms are of limited significance in hepatic clearance for lipophilic or high passive-permeability drugs. In this study, we evaluated the mechanistic role of the hepato-selective organic anion–transporting polypeptides (OATPs) 1B1/1B3 in the pharmacokinetics of compounds representing large lipophilic acid space. Intravenous pharmacokinetics of 16 compounds with molecular mass ~400–730 Da, logP ~3.5–8, and acid pKa <6 were obtained in cynomolgus monkey after dosing without and with a single-dose rifampicin–OATP1B1/1B3 probe inhibitor. Rifampicin (30 mg/kg oral) significantly ($P < 0.05$) reduced monkey clearance and/or steady-state volume of distribution (VDss) for 15 of 16 acids evaluated. Additionally, clearance of danoprevir was reduced by about 35%, although statistical significance was not reached. A significant linear relationship was noted between the clearance ratio (i.e., ratio of control to treatment groups) and VDss ratio, suggesting hepatic uptake contributes to the systemic clearance and distribution simultaneously. In vitro transport studies using primary monkey and human hepatocytes showed uptake inhibition by rifampicin (100 μM) for compounds with logP ≤6.5 but not for the very lipophilic acids (logP > 6.5), which generally showed high nonspecific binding in hepatocyte incubations. In vitro uptake clearance and fraction transported by OATP1B1/1B3 ($f_{t,OATP1B}$) were found to be similar in monkey and human hepatocytes. Finally, for compounds with logP ≤6.5, good agreement was noted between in vitro $f_{t,OATP1B}$ and clearance ratio (as well as VDss ratio) in cynomolgus monkey. In conclusion, this study provides mechanistic evidence for the pivotal role of OATP1B-mediated hepatic uptake in the pharmacokinetics across a wide, large lipophilic acid space.

SIGNIFICANCE STATEMENT

This study provides mechanistic insight into the pharmacokinetics of a broad range of large lipophilic acids. Organic anion–transporting polypeptides 1B1/1B3-mediated hepatic uptake is of key importance in the pharmacokinetics and drug-drug interactions of almost all drugs and new molecular entities in this space. Diligent in vitro and in vivo transport characterization is needed to avoid the false negatives often noted because of general limitations in the in vitro assays while handling compounds with such physicochemical attributes.

Introduction

Characterizing hepatic clearance mechanisms is of prime importance in drug discovery and development to predict systemic/target exposure and assess pharmacokinetic variability due to intrinsic and extrinsic factors, such as drug-drug interactions (DDIs), pharmacogenomics, disease state, etc. (Di et al., 2013). Preclinical and clinical data support the significance of organic anion–transporting polypeptide (OATP) 1B1 and OATP1B3 in the hepatic uptake of several high–molecular mass (MM) acidic/zwitterionic drugs (e.g., statins, sartans, and certain glinides). In addition to active uptake, hepatic metabolism and/or biliary efflux may also contribute

All authors are full-time employees of Pfizer Inc. The authors have no conflicts of interest that are directly relevant to this study. No funding was received for the work reported here.
https://doi.org/10.1124/jpet.120.000457.
[S] This article has supplemental material available at jpet.aspetjournals.org.

ABBREVIATIONS: AUC, area under the plasma concentration-time curve; CL, clearance; $CL_{h,int,Human}$, hepatic intrinsic clearance in human; $CL_{h,int,NHP}$, hepatic intrinsic clearance in NHP; DDI, drug-drug interaction; DPBS, Dulbecco's PBS; ECCS, extended clearance classification system; $f_{t,OATP1B}$, fraction transported by OATP1B; $f_{u,heps}$, fraction unbound to hepatocytes; $f_{u,p}$, fraction unbound in plasma; HBSS, Hanks' balanced salt solution; HEK, human embryonic kidney; IVIVE, in vitro–in vivo extrapolation; LC/MS, liquid chromatography tandem mass spectrometry; MM, molecular mass; NHP, nonhuman primate; NME, new molecular entity; OATP, organic anion–transporting polypeptide; PK, pharmacokinetics; PS_{inf}, uptake clearance; R_{bp}, blood-to-plasma ratio; $t_{1/2}$, half-life; VDss, steady-state volume of distribution.

to the human hepatic clearance of acidic/zwitterionic compounds (Alluri et al., 2020; Steyn and Varma, 2020). According to the extended clearance classification system (ECCS) framework, hepatic clearance of high MM (>400 Da) acids/zwitterions involves OATP1B1/1B3-mediated uptake irrespective of their passive membrane permeability (Varma et al., 2015; El-Kattan and Varma, 2018). The role of OATPs in the hepatic clearance of large hydrophilic acids—that is, with limited passive permeability (e.g., rosuvastatin, pravastatin, valsartan, etc.) —is well established. However, the relevance of uptake transporters, including OATP1B1/1B3, in determining the pharmacokinetics (PK) for highly permeable or lipophilic compounds has been consistently underappreciated. Indeed, recent US Food and Drug Administration DDI guidance recommends evaluation for OATP1B1/1B3 substrate activity in vitro and emphasizes the need for such characterization for investigational drugs with low passive membrane permeability (https://wwwfdagov/regulatory-information/search-fda-guidance-documents/vitro-drug-interaction-studies-cytochrome-p450-enzyme-and-transporter-mediated-drug-interactions). It is generally presumed that lipophilic compounds and/or compounds with high passive permeability can readily translocate across the hepatocyte basolateral membrane, and thus active transport contribution to hepatic clearance is limited.

According to ECCS, OATP1B1/1B3 likely play a key role in the hepatic clearance of not only large hydrophilic acids but also for most large lipophilic acids (Varma et al., 2015 2017a). However, there are limited clinical data to substantiate this thesis. We previously evaluated the clinical DDIs of victim drugs with the "first-choice" clinical probe inhibitor (rifampicin) recommended to investigate OATP1B1/1B3-mediated hepatic uptake activity, and clearly rifampicin caused moderate [area under the plasma concentration-time curve (AUC) ratio 2–5] and high (AUC ratio >5) interactions for class 1B and 3B drugs, whereas only no/low (AUC ratio <2) interactions for other ECCS classes [i.e., class 1A/3A—low MM (<400 Da) acids/zwitterions, and class 2/4—bases and neutral] (Varma et al., 2017a). With a limited clinical data set of only four drugs in this category (class 1B—atorvastatin, pitavastatin, glyburide, and grazoprevir), it is challenging to extend these findings to diverse chemicals in this space.

Here, we evaluated the role of OATP1B1/1B3-mediated hepatic uptake in the PK of large lipophilic acids using cynomolgus monkey [nonhuman primate (NHP)] as a preclinical model. Intravenous PK of a set of diverse acid drugs (n = 16) was studied in NHP in the presence and absence of a single dose rifampicin, an OATP1B1/1B3 inhibitor. In vitro uptake transport was characterized for these compounds using cultured monkey and human hepatocytes. Relationships between in vitro fraction transported by OATP1B ($f_{t,OATP1B}$) and the rifampicin-induced change in the intravenous clearance and steady-state volume of distribution (VDss) were assessed. Criteria for selection of compounds included molecular mass (>400 Da), lipophilicity (log P > 3.5), and acidic pKa <7.4 (i.e., anionic at physiologic pH) (Table 1). All compounds are categorized as ECCS class 1B based on their high permeability and/or extent of metabolism in human (Table 1). Compounds represent approved drugs (n = 6) and new molecular entities (NMEs) reaching clinical development (n = 10) and comprise anionic groups, including carboxylic acids, acyl sulfonamides, *N*-hetaryl sulfonamides, and tetrazoles. Chemical structures of the 16 compounds are shown in Supplemental Fig. 1. These anionic groups are commonly seen in the drugs and NMEs in therapeutic areas, such as cardiovascular, diabetes, immunology/inflammation, hepatitis C, nonalcoholic fatty liver disease, etc.

Materials and Methods

Materials. The compounds presented in this manuscript have all been reported previously. Compounds were sourced commercially when possible or prepared according to literature routes. Compounds synthesized were solubilized in DMSO, analyzed by UPLC for purity, and used for in vitro and in vivo studies when the purity was >95% (Tess et al., 2020). One of the Pfizer compounds, PF-05089771, is commercially available from MilliporeSigma (Burlington, MA). InVitroGro-HT, CP, and HI hepatocyte media were purchased from Celsis IVT (Baltmore, MD). Collagen I–coated 24-well plates were obtained from BD Biosciences (Franklin Lakes, NJ). Cryopreserved monkey hepatocytes (10106012, female) were purchased from In Vitro ADMET Laboratories LLC (Columbia, MD), and cryopreserved human hepatocytes Hu8246 (female, Caucasian, 37 years old) were purchased from Thermo Fisher Scientific (Waltham, MA). BCA protein assay kit was purchased from PIERCE (Rockford, IL). NP-40 protein lysis buffer was purchased from Thermo Fisher (Franklin, MA). Human embryonic kidney (HEK) 293 cells stably transfected with OATP1B1 were generated at Pfizer Inc. (Groton, CT). Dulbecco's modified Eagle's medium (high glucose), fetal bovine serum, nonessential amino acids, GlutaMAX, sodium pyruvate, and gentamicin were obtained from Thermo Fisher Scientific (Waltham, MA). BioCoat 96-well poly-D-lysine–treated plates were obtained from Corning Inc. (Corning, NY). Hanks' balanced salt solution (HBSS) and HEPES were obtained from Lonza (Basel, Switzerland).

In Vivo PK Studies in Cynomolgus Monkey (NHP). All procedures performed on NHPs were conducted in accordance with regulations and established guidelines and were reviewed and approved by an Institutional Animal Care and Use Committee through an ethical review process. NHP studies were conducted at Pfizer. Male cynomolgus monkeys were purchased from Covance (Princeton, NJ), Charles River Laboratories, Inc. (Wilmington, MA) or Envigo Global Services (Indianapolis, IN); subjects 3–8 years of age were used in PK studies. NHP studies used a crossover design, wherein subjects first received test compounds intravenously (i.e., control), and this was followed by a minimum 7-day washout period; then the same subjects received rifampicin dosed with test compounds (i.e., treatment). This study procedure is similar to that reported previously (Varma et al., 2017b; Kosa et al., 2018; Ufuk et al., 2018). For each study (n = 3 or 4), a cassette of two or three compounds was dosed intravenously, typically <1 mg/kg to minimize interaction between the compounds based on preliminary in vitro uptake studies using monkey hepatocytes. Each cassette was administered via intravenous infusion for 30 minutes or a bolus injection via the cephalic vein. For the treatment portion of the study, rifampicin was administered by oral gavage at a dose of 30 mg/kg (4 ml/kg) as a suspension in 0.5% aqueous methylcellulose. One hour after the rifampicin dose, test compounds were dosed intravenously. Subjects were monitored for pain or distress throughout the study, which was followed by at least daily monitoring while off study. Intravenous dosing vehicle was optimized for each cassette such that the compounds were in solution and stable for at least 24 hours. Serial blood samples were collected via the femoral vein before dosing and at predefined time points postdose. Blood samples were collected into K_2EDTA-treated collection tubes and were stored on wet ice prior to being centrifuged to obtain plasma. Each plasma sample was added to an equal volume of 0.1 M sodium acetate buffer (pH 4) and kept cold during collection, after which the plasma samples were stored frozen at −70 or −20°C. Urine samples were collected on wet ice and were added to an equal volume of 0.1 M sodium acetate buffer (pH 4.0) prior to being stored frozen at −70 or −20°C.

Liquid Chromatography Tandem Mass Spectrometry Analysis of Plasma and Urine Samples and Pharmacokinetics Analysis. Quantitation of drug substance in plasma and urine samples was done using liquid chromatography tandem mass spectrometry (LC/MS). Standard and quality-control samples prepared in blank plasma or urine with an equal volume of 0.1 M sodium acetate buffer (pH 4) were extracted in the same manner as the in-life samples. Briefly, a Waters ACQUITY ultra performance liquid chromatography system (Waters, Milford, MA) coupled to an API 4000, 5500 or 6500 triple quadrupole linear ion trap hybrid mass spectrometer equipped with either an atmospheric pressure chemical ionization or electrospray ionization source (depending upon analyte) (Applied Biosystems, MDS Sciex, Foster City, CA) was used. Chromatographic separation was accomplished using either a Waters ACQUITY UPLC BEH C18 column (1.7 μm, 2.1 × 50 mm), a Waters XSELECT CSH XP C18 column (2.5 μm, 2.1 × 50 mM), or a Waters XSelect HSS T3 column (2.5 μm, 2.0 × 30 mm) maintained at either room temperature or 45°C. The mobile phase (two solvents gradient) was optimized to achieve good separation between the analytes. Typically, solvent A was constituted of 0.025% formic acid and 1 mM NH_4OAC in water/acetonitrile (95:5 v/v), and solvent B included 0.025% formic acid and 1 mM NH_4OAC in water/acetonitrile (5:95 v/v). The gradient generally began at 3%–30% B until about 1.2 minutes, and this was followed by an increase to 50%–65% B to 1.6 minutes and then a decrease to 10%–30% B until ~1.7–1.9 minutes. Analyst 1.4.2 or 1.6.2 software (SCIEX, Framingham, MA) was used for peak integration and standard curve regression. Data were imported into Watson LIMS version 7.5 (Thermo Fisher Scientific Inc) for standard curve regression and noncompartmental pharmacokinetics parameter calculations—AUC, intravenous clearance ($CL_{total,NHP}$), volume of distribution (VD_{SS}) and effective half-life ($t_{1/2}$). The fraction of unchanged parent excreted into urine (f_e) was calculated as follows: urine concentration × total urine volume/dose. NHP hepatic clearance ($CL_{h,NHP}$) was estimated for the subsequent analyses:

$$CL_{h,NHP} = CL_{total,NHP} \cdot (1 - f_e); \text{where }, \; CL_{total,NHP} = \frac{Dose_{IV}}{AUC_{inf}} \quad (1)$$

where Dose IV is the intravenous dose. VD_{SS} and $t_{1/2}$ were calculated using the following expressions:

$$VD_{SS} = Dose \cdot \frac{AUMC}{(AUC)^2} \quad (2)$$

$$t_{1/2} = \ln(2) \cdot \frac{VD_{SS}}{CL_{total,NHP}} \quad (3)$$

wherein AUMC is the total area under the first moment of the drug concentration-time curve from time 0 to infinity.

Changes in clearance and VDss on rifampicin treatment were presented as clearance (CL) ratio and VDss ratio. Note that the f_e was less than 0.02 for all compounds in this data set (unpublished data), therefore, CL ratio can be considered as a representation of change in total clearance or hepatic clearance:

$$\text{CL ratio} = \frac{CL_{control}}{CL_{+Rifampicin}}, \text{ and VDss ratio} = \frac{VD_{ss,control}}{VD_{ss,+Rifampicin}} \quad (4)$$

The in vivo $f_{t,OATP1B}$ was calculated from intravenous clearance in the absence and presence of rifampicin:

$$f_{t,OATP1B} = \frac{CL_{control} - CL_{+Rifampicin}}{CL_{control}} \quad (5)$$

Here, subscripts "control" and "+Rifampicin" represent PK parameters in control and treatment groups, respectively. Our previous studies showed complete inhibition of OATP1B-mediated hepatic clearance of probe drugs (pitavastatin and rosuvastatin) in monkey after rifampicin 30-mg/kg oral dose (Ufuk et al., 2018).

In Vitro Uptake Studies Using Plateable Monkey and Human Hepatocytes. The cell culture and uptake study conditions with monkey and human hepatocytes were identical. The hepatic uptake assay was performed using short-term culture format as described previously with some modifications (Bi et al., 2017, 2019). Briefly, cryopreserved monkey hepatocytes (10106012, IVAL) and human hepatocytes (Hu8246) were thawed in the InVitro-HT media at 37°C, centrifuged at 50*g* for 3 minutes, and resuspended in In VitroGro-CP medium. The cells were seeded into 24-well collagen I–coated plates with 0.35×10^6 cells/well in a volume of 0.5 ml/well. The cells were cultured in the InVitro-CP media overnight (~18 hours). Plated cells were preincubated for 10 minutes at 37°C with HBSS with or without 100 μM rifampicin. The preincubation buffer was aspirated, and the uptake and inhibition reaction was initiated by addition of prewarmed buffer containing substrates (0.5 μM) with or without rifampicin (100 μM). The reactions were terminated at designated time points (0.5, 1, 2, and 5 minutes) by adding ice-cold HBSS immediately after removal of the incubation buffer. The cells were washed three times with ice-cold HBSS and lysed with 100% methanol containing internal standard, and the samples were analyzed by LC/MS (Supplemental Methods). Uptake clearance (PS_{inf}) was estimated from the initial time course (0.5–2 minutes) by linear regression (Bi et al., 2017, 2019). The in vitro $f_{t,OATP1B}$ was calculated from PS_{inf} measured in the absence and presence of 100 μM rifampicin. At this concentration, rifampicin completely inhibits OATP1B1 and OATP1B3 in vitro (Bi et al., 2017, 2019):

$$f_{t,OATP1B} = \frac{PS_{inf,control} - PS_{inf,+Rifampicin}}{PS_{inf,control}} \quad (6)$$

Measurement of Fraction Unbound in Human Hepatocytes Using Equilibrium Dialysis. The 96-well equilibrium dialysis (HTD 96) device and cellulose membranes with molecular mass cutoff of 12–14 K were from HTDialysis, LLC (Gales Ferry, CT). Velocity V11 peelable seals were obtained from BD Falcon (Bedford, MA). Deep 96-well plates of 1.2-ml blocks were from Axygen Scientific Inc (Union City, CA). Orbital shaker and vortex mixer were from VWR (Radnor, PA). The details of the experiments measuring fraction unbound to hepatocytes ($f_{u,heps}$) have been described previously (Riccardi et al., 2018).

Cryopreserved human hepatocytes were thawed and added into HBSS to make a final concentration of 0.7×10^6 cells/ml concentration matrix (similar cell density as in hepatocyte uptake studies). The dialysis membranes were prepared a day before the experiment. The cellulose membranes were immersed in deionized water for 15 minutes followed by 15 minutes in 30% ethanol/deionized water, and then they were left overnight in DPBS. A 150-μl aliquot of hepatocyte matrix spiked with 1 μM compound was added to one side of the chamber (donor), and 150 μl of DPBS was added to the other side of the dialysis membrane (receiver). The equilibrium dialysis device was sealed with a breathable easy gas permeable membrane and was placed on an orbital shaker at 200 rpm at 37°C in quadruplicate for 6 hours. After incubation, aliquots of 45 μl of dialyzed DPBS and 15 μl hepatocyte matrix were matrix-matched and quenched with cold acetonitrile containing internal standard (carbamazepine or tolbutamide) to precipitate the proteins. The plates were sealed and mixed with a vortex mixer for 1 minute and then centrifuged at 2000 × g at room temperature for 5 minutes. The supernatant was transferred to a new deep well block, sealed, and subsequently analyzed using LC/MS (Supplemental Methods). $f_{u,heps}$ was than calculated as ratio of receiver to donor area signal (Riccardi et al., 2018).

In Vitro–In Vivo Extrapolation of Hepatic Clearance. Assuming hepatic uptake as the rate-determining step in the overall hepatic clearance, IVIVE was evaluated using the in vitro apparent total PS_{inf} obtained after monkey or human hepatocyte incubations. IVIVE was assessed without and with correction for $f_{u,heps}$. The $f_{u,heps}$

values were obtained using human hepatocytes and were assumed to be same for monkey hepatocytes. Standard physiologic scalars were used to scale up in vitro data: 1×10^6 hepatocytes/mg-measured protein, 120×10^6 hepatocytes/g-liver, 21 g-liver/kg-body weight (Davies and Morris, 1993; Hosea et al., 2009).

In vivo (observed) hepatic intrinsic clearance ($CL_{int,h}$) was calculated using the well stirred clearance model (eq. 7):

$$CL_{int,h} = \frac{R_{bp} \cdot Q_h \cdot CL_h}{(R_{bp} \cdot f_{u,p} \cdot Q_h - f_{u,p} \cdot CL_h)} \quad (7)$$

wherein CL_h is hepatic clearance (total intravenous clearance minus renal clearance), R_{bp} is blood-to-plasma ratio, $f_{u,p}$ is fraction unbound in plasma, and Q_h is hepatic blood flow (human, 20; NHP 44 ml/min per kilogram).

Results

Effect of Rifampicin on Intravenous PK of Large Lipophilic Acids in Cynomolgus Monkey. A single dose rifampicin (30 mg/kg orally administered) significantly altered plasma exposure of almost all the large lipophilic acids dosed intravenously in cynomolgus monkey (Fig. 1). Indeed, 14 of 16 compounds evaluated showed reduction in the intravenous clearance by more than 2-fold (Table 2). CL ratio (i.e., ratio of hepatic clearance in control to rifampicin treatment groups, eq. 4) ranged from unity (epristeride) to about 27.7 ± 9.0 (MK-3577), with a geometric mean of 4.0 across the 16 compounds. VDss also decreased considerably after rifampicin dosing compared with control, and a significant linear relationship was observed between CL ratio and VDss ratio (i.e., ratio of VDss in control to rifampicin treatment groups) (Fig. 2A). Interestingly, epristeride, which showed no change in clearance, had a marked increase in VDss (~4×). On the other hand, glyburide showed a small change in VDss (~1.5×) in relation to the large change in clearance (~13×). A significant linear relationship was also observed for the $VDss_{control}$ (volume in control group) and VDss ratio, implying that the change in VDss is higher for acids with high $VDss_{control}$ (Fig. 2D). In the control group, a trend for an increase in VDss with an increase in clearance was apparent, although a linear relationship was not statistically significant ($P > 0.05$) (Fig. 2B). Also, a clear correlation between $CL_{control}$ and CL ratio was not seen (Fig. 2C). On the other hand, effective $t_{1/2}$ increased (by >2-fold) when dosed with rifampicin for only five compounds (montelukast, gliquidone, verlukast, glyburide, and MK-3577) (Table 2). Moreover, based on the plasma concentration-time profiles (Fig. 1), it is apparent that the terminal $t_{1/2}$ of the lipophilic acids remained similar or decreased after rifampicin treatment.

Comparison of In Vitro Uptake Transport in Monkey and Human Hepatocytes. Using short-time cultured (6 hours) monkey and human hepatocytes, uptake transport of the 16 compounds was measured in the absence and presence of 100 μM rifampicin (Fig. 3; Table 3). Firstly, total PS_{inf} is comparable between human and monkey hepatocytes, with most of the compounds falling within 3-fold error. LY2393910 showed low PS_{inf} (~6.6 ml/min per kilogram), whereas pitavastatin and irbesartan showed higher uptake clearance (~300 ml/min per kilogram) in monkey hepatocytes. Rifampicin did not inhibit uptake of a few compounds (gliquidone, GSK269984A, LY2409021, MK-0893, and montelukast) in both human and monkey hepatocytes. Interestingly, these compounds are relatively more lipophilic (logP >6.5). LY2393910, also with logP >6.5, showed about 25% reduced uptake in the presence of rifampicin. However, all others (logP <6.5) with the exception of epristeride showed significant active uptake in both human and monkey hepatocytes. The in vitro $f_{t,OATP1B}$, which was estimated assuming 100 μM rifampicin inhibits OATP1B1/1B3 completely, was comparable between human and monkey hepatocytes (Fig. 3B).

In vitro substrate studies using HEK293 cells demonstrated OATP1B1-mediated transport for all compounds with logP <6.5 except epristeride (Table 3). However, consistent with the hepatocyte uptake data, acids with logP >6.5 could not be recognized as OATP1B1 substrates under the current experimental conditions. We additionally studied OATP1B1 inhibition in transfected HEK293 cells, and notably, all 16 compounds inhibited OATP1B1-mediated rosuvastatin transport at 10 μM concentration, suggesting affinity to the transporter protein (Table 3).

In Vitro–In Vivo Extrapolation of Uptake Clearance to Predict Monkey and Human Hepatic Clearance. In vitro apparent PS_{inf} measured in monkey and human hepatocytes was used to predict in vivo hepatic intrinsic clearance in NHP ($CL_{h,int,NHP}$) and human ($CL_{h,int,Human}$), respectively, assuming uptake as the rate-determining process to the overall clearance (Fig. 4). Direct extrapolation of monkey hepatocyte data (i.e., PS_{inf}) yielded considerable underprediction; particularly, in vitro PS_{inf} was several-fold lower than the observed $CL_{h,int,NHP}$ for all acids with logP >6.5 (Fig. 4A). Corresponding predictions of human hepatic clearance from in vitro PS_{inf} showed similar underprediction, although the bias was relatively small.

Given the lipophilic and sticky nature of the compounds in this space, we measured $f_{u,heps}$ via equilibrium dialysis methodology using a human hepatocyte homogenate prepared with similar cell density as employed in the plateable human hepatocyte/plateable monkey hepatocyte assay. Four of the six compounds with logP >6.5 showed $f_{u,heps}$ <0.004, suggesting high nonspecific binding to hepatocytes in the in vitro experimental conditions (Table 3). Other compounds showed $f_{u,heps}$ generally in the range of 0.20–0.70. Previous studies from our laboratory suggested that the measured fraction unbound values in human and monkey liver tissues are largely similar (Ryu et al., 2020). Therefore, the $f_{u,heps}$ values obtained using human hepatocytes were assumed to be same for monkey hepatocytes. Correction for the nonspecific binding in the incubations (i.e., use of $PS_{inf}/f_{u,heps}$) generally improved the IVIVE (Fig. 4, A and B). Nevertheless, systemic underprediction of hepatic intrinsic clearance was still apparent in the case of NHP scaling, in which predicted clearance of 10 of 16 compounds were <3-fold of observed values. However, in case of human clearance, about 57% of the predictions (8 of 14) were within 3-fold error when corrected for $f_{u,heps}$. Underprediction in human clearance after correcting for hepatocyte binding was noted only for dexloxiglumide, glyburide, and PF-05241328, whereas three compounds showed overprediction (>3-fold).

A cross-species empirical scaling approach, as suggested previously (De Bruyn et al., 2018), was assessed to predict human clearance. In this case, the compound-specific scaling factors in NHP (SF, ratio of $CL_{h,int,NHP}$ to monkey $PS_{inf}/f_{u,heps}$)

TABLE 1
Summary of physicochemical properties, in vitro data, and observed hepatic clearance in cynomolgus monkey and human of the 16 compounds

Compound	Code	Acid pKa[a]	Permeability[b]	MM	$LogD_{7.4}$[c]	LogP	NHP R_{bp}	NHP $f_{u,p}$[d]	NHP Observed Hepatic Clearance	Human R_{bp}	Human $f_{u,p}$[d]	Human Observed Hepatic Clearance[e]
			10^{-6} *cm/s*	*Da*					*ml/min per kilogram*			*ml/min per kilogram*
Danoprevir	Dan	5.3[f]	2.5[g]	731.8	1.3	3.3	0.73[h]	0.085	23.59	0.73	0.072	10.8
Dexloxiglumide	Dex	4.2	4.6[g]	461.4	1.5	4.4	0.60	0.00771	1.25	0.56	0.00969	3.3
Epristeride	Epi	4.6	20.0	399.6	3.4	5.1	0.55	0.00917	1.43	0.55	0.0138	0.33
Gliquidone	Gli	5.3[f]	5.7	527.6	2.6	6.7	0.62[h]	0.0015	3.33	0.62	0.0035	0.96
Glyburide	Gly	5.3	14.0	494.0	2.1	4.8	0.61	0.00179	4.58	0.57	0.00217	1.23
GSK269984A	Gsk	5.3	12.0	406.2	2.1	6.8	0.56	0.00288	17.1	0.65	0.0024	2.0
Irbesartan	Irb	3.5	8.6	428.5	1.3	4.1	0.55	0.0126	10.86	0.60	0.0155	2.1
LY2393910	Ly23	3.8	4.4[g]	556.0	4.8	7.4	0.55	0.0003	8.65	0.65	0.0003	N/A
LY2409021	Ly24	4.4	4.5[g]	555.6	4.8	8.1	0.82	0.000056	1.83	0.61	0.000036	0.078[e]
MK-0893	Mk8	5.6	9.9	588.5	4.0	8.8	0.55[h]	0.0001	7.12	0.55	0.0001	N/A
MK-3577	Mk3	4.1	4.4[g]	521.0	3.5	6.3	0.95	0.000228	25.3	0.55	0.000249	4.9[e]
Montelukast	Mon	5.4	12.5	586.2	5.1	8.5	0.70	0.0002	1.25	0.66	0.0002	0.57
PF-05089771	PF771	6.0	7.1	500.4	2.3	4.3	0.60[h]	0.00164	1.62	0.60	0.0015	0.59
PF-05241328	PF328	3.6	16.6	436.9	2.0	4.2	0.75	0.00199	25.0	0.56	0.0019	5.7
Pitavastatin	Pit	4.7	8.5	421.5	1.3	3.5	0.65	0.0263	19.8	0.65	0.008	5.6
Verlukast	Ver	4.4	8.5	515.1	1.5	5.3	0.58	0.00116	8.5	0.66	0.00142	0.91

[a]pK_a values were determined by electrophoresis as previously described (Shalaeva et al., 2008).
[b]P_{app}, apparent permeability measured using low-efflux Madin-Darby canine kidney cell line. Permeability experiments were conducted with a modification to a previously reported methodology (Di et al., 2011; Varma et al., 2012). Modification included addition of 0.4% bovine serum albumin to the receiver compartment to minimize nonspecific binding and thus maximize recover the analyte from the wells once permeated across the cell monolayers. Note that these lipophilic compounds often show nonspecific binding in the in vitro assays, and our preliminary data suggested underestimation of permeability and low assay recoveries when using conventional permeability protocols (i.e., no serum albumin in receiver).
[c]LogD was measured at pH 7.4 using the previously described shake-flask method (Stopher and McClean, 1990).
[d]$f_{u,p}$ was measured by equilibrium dialysis as previously described (Riccardi et al., 2019).
[e]Human hepatic clearance was obtained after intravenous dosing except in case of LY2409021 and MK-3577, in which clearance was estimated from oral clearance assuming Fa × Fg as one (see Tess et al. (2020)). N/A, not available. References for observed human hepatic clearance are provided in Supplemental Table 1.
[f]pK_a, experimental data not available, and values were obtained from MoKa 3.2.1. calculator; pKa of danoprevir was taken from (Jiang et al., 2014).
[g]Compound classified as ECCS class 1B, although the measured transcellular passive permeability is lower than the cutoff value of 5×10^{-6} cm/s on the basis of extensive metabolism in vivo (Tess et al., 2020).
[h]NHP R_{bp} was assumed to be similar to human R_{bp}, in which in vitro data were not available.

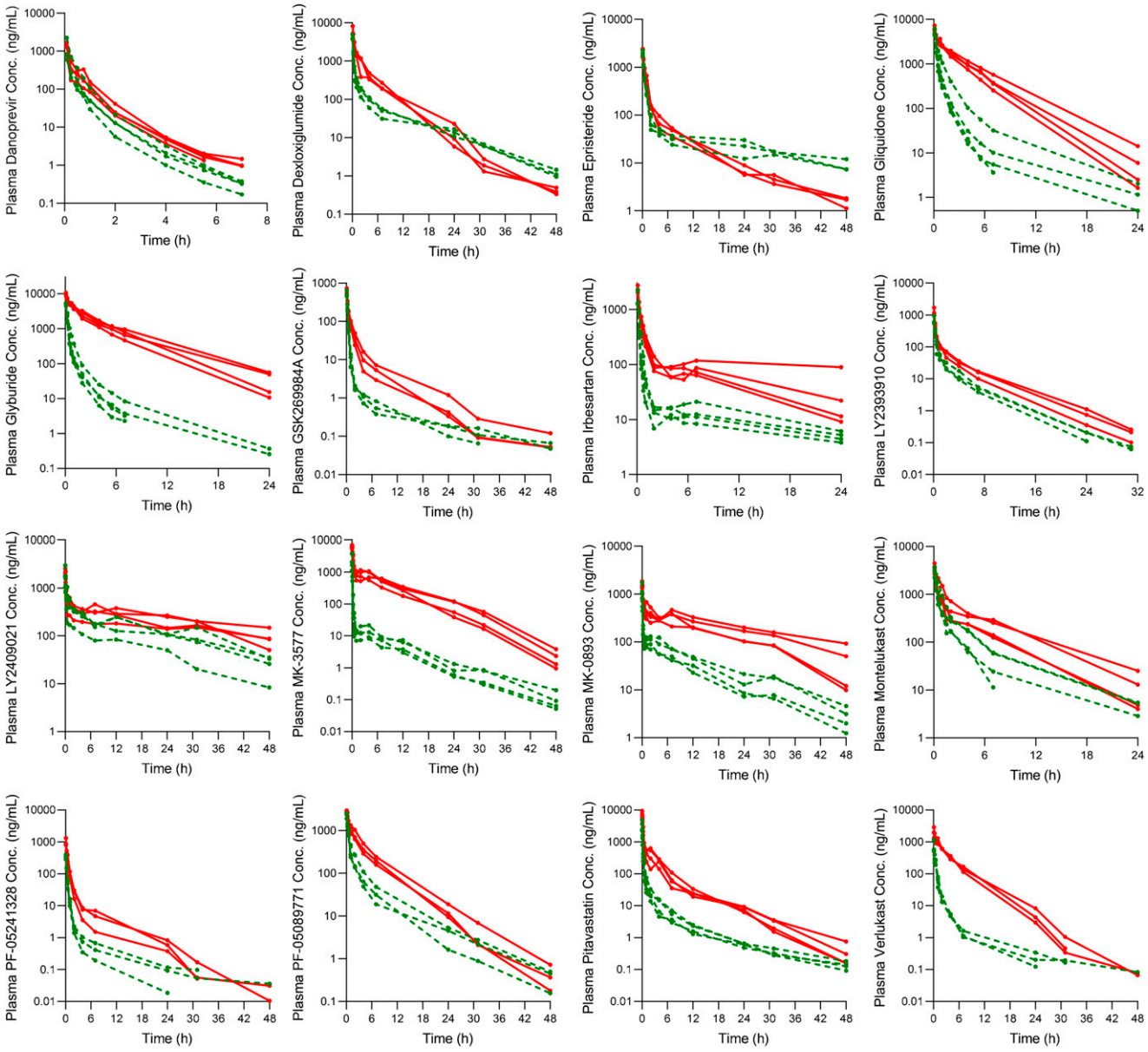

Fig. 1. Intravenous pharmacokinetics of 16 large lipophilic acids in cynomolgus monkey when dosed without and with single-dose oral rifampicin. Data represent plasma concentration-time profiles in individual animals in the control (dashed curves) and rifampicin treatment (solid curves) groups (n = 3 to 4). Same subjects were dosed in the control and treatment groups with at least 7-day washout period.

were used to scale human $PS_{inf}/f_{u,heps}$ to predict $CL_{h,int,Human}$. Cross-species scaling generally overpredicted clearance (Fig. 4C). Given that the in vitro PS_{inf} were similar in human and monkey hepatocytes (Fig. 3A), the predicted $CL_{h,int,Human}$ values obtained by cross-species scaling were very consistent with the observed $CL_{h,int,NHP}$ (Fig. 4D).

Comparison of Fraction Transported by OATP1B In Vitro and In Vivo. The in vitro fraction of compound transported by OATP1B1/1B3 ($f_{t,OATP1B}$) in monkey and human hepatocytes was estimated by measuring uptake in the absence and presence of rifampicin (100 μM). Our previous studies have shown that rifampicin at this concentration abates OATP1B1/1B3 activity (Bi et al., 2017, 2019). Cellular accumulation of the six compounds with logP >6.5 was not affected by rifampicin in vitro, although all of these compounds had CL ratio between 2 and 6 in vivo (Fig. 5A). Note that these compounds also showed high nonspecific binding to the hepatocytes ($f_{u,heps}$ <0.004). For acids with logP <6.5, a good correlation was observed between the $f_{t,OATP1B}$ obtained using monkey hepatocytes and the in vivo CL ratio with two exceptions (glyburide and verlukast). The correlation can generally be described by the expression, CL ratio = 1/(1–$f_{t,OATP1B}$), which relies on the uptake-determined clearance of the substrate drugs and the complete inhibition of OATP1B activity by rifampicin administered in vivo. Indeed, the rifampicin unbound plasma concentrations in cynomolgus monkey after 30-mg/kg oral dose well exceeded the concentration above 90% inhibition of OATP1B1 over the 12 hours postdose (Supplemental Fig. 2). Interestingly, there was an exceptional correlation between $f_{t,OATP1B}$ and NHP VDss ratio (Fig. 5B). Finally, a comparison of $f_{t,OATP1B}$ measured using human hepatocytes and CL ratio or VDss ratio in NHP also

TABLE 2
Pharmacokinetic parameters of large lipophilic acids in cynomolgus monkey when dosed in the absence and presence of single-dose rifampicin (30 mg/kg)

Compound	n	$CL_{u,Control}$ (Mean ± S.D.)[a]	$CL_{u,+Rifampicin}$ (Mean ± S.D.)	$VDss_{Control}$ (mean ± S.D.)	$VDss_{+Rifampicin}$ (Mean ± S.D.)	Effective $t_{1/2,Control}$ (Mean)	Effective $t_{1/2,+Rifampicin}$ (Mean)	CL Ratio[b] (Mean ± S.D.)	VDss ratio[b] (Mean ± S.D.)	$t_{1/2,+Rifampicin}/t_{1/2,Control}$ ratio (Mean)
		ml/min per kilogram	*ml/min per kilogram*	*l/kg*	*l/kg*	*h*	*h*			
Danoprevir	4	23.59 ± 9.15	15.60 ± 5.02	0.61 ± 0.30	0.53 ± 0.18	0.3	0.4	1.5 ± 0.5	1.2 ± 0.7	1.3
Dexloxiglumide	3	1.25 ± 0.21	0.40 ± 0.08**	0.36 ± 0.12	0.08 ± 0.02*	3.3	2.3	3.1 ± 0.4	4.4 ± 1.0	0.7
Epristeride	3	1.43 ± 0.17	1.39 ± 0.16	1.48 ± 0.29	0.37 ± 0.10**	12.0	3.1	1.1 ± 0.3	4.1 ± 1.0	0.3
Gliquidone	4	3.33 ± 1.10	0.61 ± 0.09**	0.17 ± 0.03	0.12 ± 0.00*	0.6	2.3	5.5 ± 1.7	1.4 ± 0.3	3.9
Glyburide	4	4.58 ± 0.95	0.37 ± 0.06***	0.13 ± 0.02	0.08 ± 0.01**	0.3	2.6	12.6 ± 2.6	1.6 ± 0.2	7.8
GSK269984A	3	17.10 ± 1.94	7.49 ± 1.44**	1.37 ± 0.64	0.95 ± 0.16	0.9	1.5	2.3 ± 0.2	1.4 ± 0.6	1.6
Irbesartan	4	10.86 ± 2.74	3.38 ± 0.68**	5.30 ± 1.91	1.03 ± 0.21**	5.6	3.5	3.2 ± 0.4	5.6 ± 3.0	0.6
LY2393910	3	8.65 ± 1.28	4.01 ± 0.55**	0.90 ± 0.16	0.54 ± 0.08*	1.2	1.6	2.2 ± 0.1	1.7 ± 0.3	1.3
LY2409021	4	1.83 ± 1.08	0.74 ± 0.14*	1.91 ± 0.82	1.52 ± 0.65	12.1	23.7	2.4 ± 1.2	1.3 ± 0.1	1.9
MK-0893	4	7.12 ± 2.19	1.16 ± 0.41**	4.72 ± 0.91	1.22 ± 0.18***	7.7	12.1	6.3 ± 0.8	3.9 ± 0.8	1.6
MK-3577	4	25.30 ± 7.55	0.93 ± 0.23***	5.16 ± 2.24	0.41 ± 0.10**	2.4	5.1	27.7 ± 9.0	13.6 ± 7.9	2.2
Montelukast	4	1.25 ± 0.41	0.64 ± 0.24*	0.16 ± 0.05	0.16 ± 0.04	1.4	2.9	2.0 ± 0.3	1.0 ± 0.5	2.0
PF-05089771	3	1.62 ± 0.39	0.51 ± 0.08**	0.28 ± 0.08	0.12 ± 0.01*	2.0	2.7	3.2 ± 0.3	2.4 ± 0.7	1.4
PF-05241328	3	25.00 ± 2.42	6.09 ± 1.45***	1.60 ± 0.91	0.50 ± 0.02	0.7	0.9	4.2 ± 0.6	3.2 ± 1.8	1.3
Pitavastatin	4	19.80 ± 2.25	3.99 ± 1.52***	1.53 ± 0.43	0.53 ± 0.34*	0.9	1.5	5.3 ± 1.2	3.5 ± 1.3	1.7
Verlukast	3	8.50 ± 1.52	0.66 ± 0.04***	0.65 ± 0.35	0.14 ± 0.03	0.9	2.4	12.9 ± 1.6	4.5 ± 1.8	2.8

n, number of animals per group.
[a]Mean values are same as in Table 1.
[b]For ratio calculations (eq. 4), each cynomolgus monkey served as its own control.
*$P < 0.05$, **$P < 0.01$, ***$P < 0.001$, significantly different from the control group (paired t test).

showed good concordance, although there was a relatively higher scatter (Supplemental Fig. 3).

Discussion

Toward the primary objective, this study demonstrates the pivotal role of OATP1B1/1B3-mediated hepatic uptake in determining the PK of large lipophilic carboxylic acids and the related bioisosteres, and the findings can be generalized across a broad physicochemistry (MM ~400–730 Da, logP ~3.5–8, and acid pKa < 6.0; typically ECCS class 1B compounds). We evaluated 16 compounds (six marketed drugs and 10 NMEs that reached clinical development) in vivo in the cynomolgus monkey and in vitro using primary monkey and human hepatocytes. Single-dose rifampicin (prototypical OATP1B1/1B3 inhibitor) significantly altered the plasma concentrations of 15 of the 16 large lipophilic acids dosed intravenously in cynomolgus monkey. Additionally, there was a good correlation between the magnitude of change in clearance (CL ratio) versus the change in VDss (VDss ratio). These findings clearly imply that the rifampicin-induced change in PK of large lipophilic acids is associated with the inhibition of OATP1B1/1B3-mediated hepatic uptake. In the majority of cases, the in vivo findings are well substantiated by the in vitro data, wherein a good agreement was observed between in vitro and in vivo $f_{t,OATP1B}$ in NHP. These findings are of clinical relevance in this broader physicochemical space, especially since many of these compounds were not tested for the relevance of OATP1B1/1B3 in clinical studies. To our knowledge, clinical DDI data with OATP1B probe inhibitors (e.g., rifampicin and cyclosporine) are available only for danoprevir (Brennan et al., 2015), glyburide (Zheng et al., 2009), and pitavastatin (Prueksaritanont et al., 2014), wherein the human PK of these substrate drugs was modulated by an inhibitor. For the other compounds, preclinical data presented in this study may provide basis for further clinical investigation and/or improved mechanistic rationalization of their human PK variability because of intrinsic and extrinsic factors (e.g., age, disease state, DDIs, etc.).

VDss is generally thought to be determined by the physicochemical properties (e.g., logP and ionization) of compounds (Rodgers and Rowland, 2007; Smith et al., 2015). Carboxylic acids and related bioisosteres (acid pKa <6.0) are anionic at physiologic pH and have limited lipid partitioning that restricts the compound to circulating blood, and they are therefore expected to have low VDss (<0.2 l/kg). NHP VDss of the compounds evaluated in this study ranged from 0.13 l/kg (glyburide) to about 5 l/kg (irbesartan, MK-0893, MK-3577), which was clearly reduced on rifampicin treatment. Notably, compounds with high VDss showed relatively higher VDss ratio (Fig. 2D). A linear correlation between the CL ratio and VDss ratio further signifies the role of hepatic uptake in the PK of these compounds. In contrast, inhibition of hepatic metabolism or biliary secretion alone typically does not alter VDss (Grover and Benet, 2009). Overall, the data suggest that large lipophilic acids may show larger-than-expected VDss primarily driven by their transport rates across the basolateral membrane of hepatocytes and that the liver acts as a major distribution compartment for such compounds. Accounting for such transporter-mediated distribution should further help predict plasma concentration-time profiles and dose optimization in drug discovery.

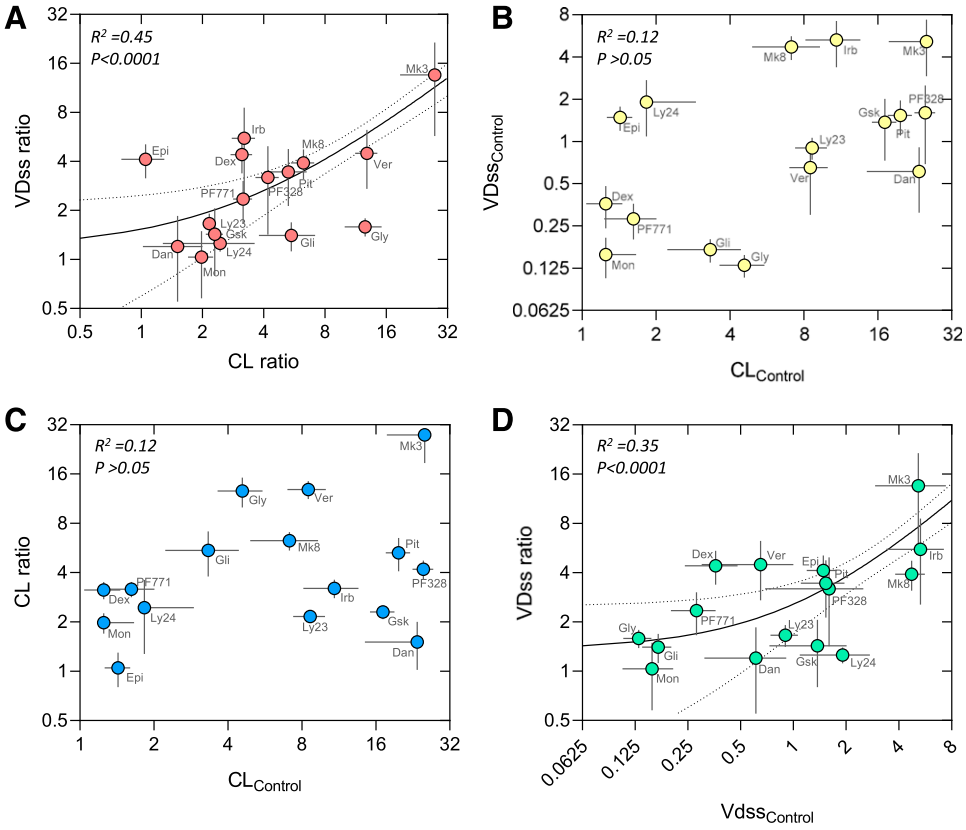

Fig. 2. Inter-relationship between cynomolgus monkey pharmacokinetic parameters. (A) Correlation between change in clearance and VDss of large lipophilic acids on single-dose rifampicin treatment in cynomolgus monkey. (B) Correlation between clearance and VDss in the control group. (C) Correlation between clearance in the control group and change in CL ratio. (D) Correlation between VDss in the control group and change in VDss on rifampicin treatment (VDss ratio). Data points depict mean ± S.D. (n = 3 to 4). When presented, curves represent linear regression fit to the observed data and 95% confidence interval. R^2, linear regression coefficient. Statistical significance of the linear relationship was tested at P value 0.05. Data points are labeled with compound code (Table 1).

We employed cynomolgus monkey, which has been shown as a useful animal model for the assessment of OATP1B-mediated disposition and drug-drug interactions due to the high degree of gene and amino acid sequence identity between NHP and human orthologs (>93% for OATP1B uptake transporters) (Ebeling et al., 2011; Shen et al., 2013). Recent studies have also drawn several parallels at the level of functional activity, including the following: 1) The mechanisms of transporter-mediated drug-drug interactions in humans and NHPs appear to be comparable (Shen et al., 2013; Takahashi et al., 2013; Shen et al., 2015; De Bruyn et al., 2018; Kosa et al., 2018; Ufuk et al., 2018; Liao et al., 2019), 2) in vivo studies showed similarity in biliary excretion (Kimoto et al., 2017) and handling of some endogenous OATP1B biomarkers (Chu et al., 2015; Shen et al., 2016; Thakare et al., 2017), 3) members of monkey cytochrome P450 exhibit >90% homology in amino acid sequences with corresponding human CYPs and similar hepatic metabolic activity in vitro and in vivo (Iwasaki and Uno, 2009), and 4) human hepatic clearance was shown to be well predicted based on the species scaling of monkey hepatic clearance for a large set of OATP substrates (Tess et al., 2020). The current in vitro data (PS_{inf} and % active uptake) also corroborate similarities in human and NHP transport mechanisms and thus suggest the latter as a valuable preclinical model. On the other hand, rodents do not express key human hepato-selective OATPs (OATP1B1/1B3) but instead express orthologs with only ~70% sequence similarity in liver. Such differences can present uncertainty when projecting disposition mechanisms in human (Chu et al., 2013; Tess et al., 2020). Alternatively, humanized rodent models (Oatp1a/1b knockout and OATP1B1/1B3 knock in) are emerging as useful tools for studying the role of these transporters in drug disposition (Higgins et al., 2014; Salphati et al., 2014). However, some reports showed limited in vivo function for probe substrates

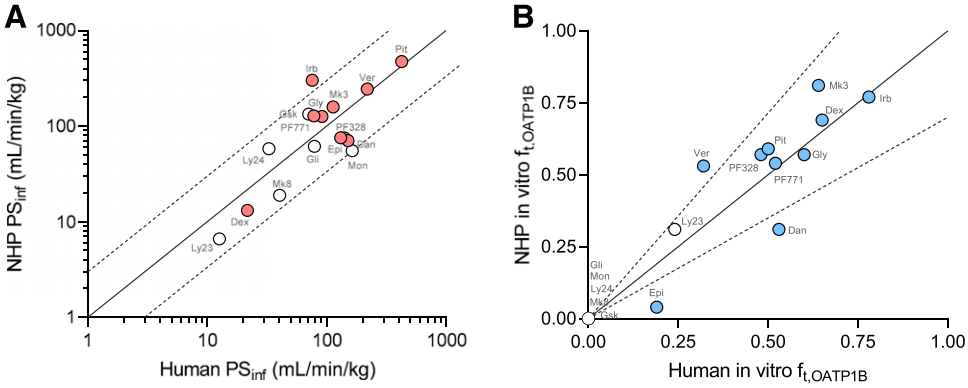

Fig. 3. Comparison of in vitro uptake in human and monkey cultured hepatocytes. (A) Comparison of total uptake clearance in human vs. monkey hepatocytes. (B) Comparison of percent active uptake in human vs. monkey hepatocytes. Data points represent mean values for compounds with log P ≤6.5 (closed points) and log P >6.5 (open points). Variability in uptake parameters for each compound is presented in Table 3. Diagonal lines represent unity and ±3-fold error or ±20% error in case of percent active uptake. Data points are labeled with compound code (see Table 1).

TABLE 3
In vitro transport activity of 16 large lipophilic acids in the OATP1B1-transfected HEK293 cells and monkey and human primary hepatocytes

Compound	OATP1B1 Uptake Ratio[a] [Mean (%CV)]	OATP1B1 Inhibition[b] (Mean)	Human PS_{inf}[c] [Mean (%CV)]	Human $PS_{inf,+Rif}$[c] [Mean (%CV)]	Monkey PS_{inf}[c] [Mean (%CV)]	Monkey $PS_{inf,+Rif}$[c] [Mean (%CV)]	$f_{u,heps}$[d] [Mean (%CV)]	Human In Vitro $f_{t,OATP1B}$ (Mean)	Monkey In Vitro $f_{t,OATP1B}$ (Mean)	Monkey In Vivo $f_{t,OATP1B}$ (Mean)
		% inhibition at 10 μM	*ml/min per kilogram*	*ml/min per kilogram*	*ml/min per kilogram*	*ml/min per kilogram*				
Danoprevir	9.6 (6)*	98	151.2 (7)	70.6 (9)*	70.6 (11)	48.9 (11)*	0.30 (9)	0.53	0.31	0.34
Dexloxiglumide	2.0 (6)*	82	21.7 (27)	7.6 (22)*	13.1 (23)	4.0 (14)*	0.73 (22)	0.65	0.69	0.68
Epristeride	0.8 (4)	52	141.6 (9)	115.4 (17)	75.1 (11)	71.8 (15)	0.48 (9)	0.19	0.04	0.03
Gliquidone	1.0 (2)	99	78.9 (26)	137.1 (31)	61.5 (20)	102.6 (23)	0.51 (4)	0	0	0.82
Glyburide	2.2 (6)*	95	91.5 (13)	37.0 (27)*	126.3 (8)	54.2 (11)*	0.51 (17)	0.60	0.57	0.92
GSK269984A	0.8 (2)	100	70.5 (14)	88.2 (13)	133.8 (19)	134.6 (24)	0.21 (5)	0	0	0.56
Irbesartan	3.1 (4)*	79	75.6 (10)	16.6 (20)*	302.4 (18)	70.6 (16)*	0.67 (5)	0.78	0.77	0.69
LY2393910	0.9 (11)	42	12.6 (18)	9.6 (37)	6.6 (33)	4.5 (43)	0.00024 (14)	0.24	0.31	0.54
LY2409021	1.1 (12)	54	32.8 (17)	100.8 (16)	58.0 (36)	118.4 (26)	0.00078 (15)	0	0	0.60
MK-0893	1.1 (7)	61	40.3 (26)	75.6 (21)	18.9 (31)	32.8 (37)	0.00058 (17)	0	0	0.84
MK-3577	3.1 (4)*	83	113.4 (10)	40.3 (16)*	158.8 (10)	30.2 (23)*	0.0037 (17)	0.64	0.81	0.96
Montelukast	1.0 (3)	99	163.8 (52)	186.5 (36)	55.4 (31)	141.1 (38)	0.0037 (13)	0	0	0.49
PF-05089771	1.6 (4)*	95	78.1 (29)	37.8 (24)*	128.0 (10)	59.5 (6)*	0.36 (12)	0.52	0.54	0.69
PF-05241328	2.2 (2)*	86	131.0 (27)	68.5 (13)*	75.6 (9)	32.8 (16)*	0.21 (8)	0.48	0.57	0.76
Pitavastatin	9.9 (2)*	96	425.9 (12)	214.2 (15)*	473.8 (18)	196.6 (15)*	0.67 (16)	0.50	0.59	0.80
Verlukast	1.5 (7)*	98	219.2 (8)	148.7 (8)*	244.4 (6)	115.9 (18)*	0.20 (14)	0.32	0.53	0.92

[a]Ratio of cell accumulation in HEK-OATP1B1 cells to HEK–wild-type cells ($n = 6$). *$P < 0.05$, uptake significantly higher in transfect cells compared with wild-type cells (unpaired t test).
[b]Inhibition of OATP1B1-mediated uptake of rosuvastatin in transfected HEK cells. Value represent mean percent inhibition at 10 μM conc. ($n = 3$). Variability in the inhibition studies was within 10% coefficient of variance (not shown).
[c]Apparent uptake clearance measured in human or monkey hepatocytes in the absence (PSinf) and presence (PSinf,+Rif) 100 μM rifampicin. Values represent mean and percent coefficient of variance estimated from two to four independent experiments, each experiment run in triplicate. *$P < 0.05$, uptake significantly inhibited by rifampicin (unpaired t test).
[d]$f_{u,heps}$ was measured by equilibrium dialysis using human hepatocytes (see *Materials and Methods*).

(e.g., pitavastatin and rosuvastatin) in humanized OATP1B1 mice, suggesting challenges in the translation of the findings from humanized mice to humans (Salphati et al., 2014). Further understanding and refinement are therefore required to employ these models for characterizing human hepatic uptake.

Our secondary objective was to provide in vitro data (e.g., studies using transfected cell and monkey and human hepatocytes) in support of the in vivo findings in NHP. Generally, a good agreement was observed between in vitro and in vivo $f_{t,OATP1B}$ in NHP for compounds with logP ≤6.5 (Fig. 5). In this study, some very lipophilic acids (logP >6.5; e.g., montelukast, LY2409021, MK-0893) did not produce expected results in the in vitro assays (hepatocyte uptake, OATP1B1 substrate assay, etc.). Also, the presence of rifampicin in the incubations did not reduce cellular accumulation for these compounds, although a clear in vivo signal was seen in cynomolgus monkey with CL ratio reaching as high as 6.3 (MK-0893). It is noteworthy that these compounds show high binding to hepatocytes ($f_{u,heps} <$ 0.004), and under such conditions the in vitro assays may not have the fidelity to distinguish active uptake from nonspecific cell binding. It is worth noting that highly lipophilic compounds can be generally problematic to study absorption, distribution, metabolism, and excretion properties in vitro, including permeability, plasma protein binding, metabolism, and transport kinetics (Press and Di Grandi, 2008). This may be attributed to one or several experimental reasons, including nonspecific binding to the cell surface and assay apparatus, etc. (associated with high lipophilicity). Therefore, additional diligence is necessary in characterizing the uptake mechanism in this space to avoid unexpected clinical readouts. In particular, for compounds in the current physicochemical space (MM ~400–730 Da and logP ~3.5–8, acid pKa <6.0), if in vitro studies do not provide appropriate guidance, preclinical in vivo studies may support the qualitative assessment of the contribution of hepatic uptake to overall clearance, which in turn may provide impetus for early clinical assessment of inhibitor (e.g., rifampicin) and genotype impact on pharmacokinetics.

Considerable underprediction was noted in the IVIVE of NHP and human hepatic clearance when using in vitro PS_{inf} directly and scaled assuming hepatic uptake as the rate-determining process to the overall clearance in both species. Correction for the binding to hepatocytes ($f_{u,heps}$) markedly improved the predictions, although the overall performance may still be suboptimal for prospective predictions (Fig. 4). Potential sources for the IVIVE inconsistencies in scaling uptake clearance are discussed in several previous reports (Watanabe et al., 2009; Jones et al., 2012; (Ménochet et al., 2012); Varma et al., 2014; Kimoto et al., 2017). Additionally, recent studies have suggested "albumin-mediated uptake," wherein presence of albumin/plasma in the in vitro incubations could improve IVIVE for OATP1B substrates (Bowman and Benet, 2018; Miyauchi et al., 2018; Bteich et al., 2019; Kim et al., 2019; Riccardi et al., 2019; Liang et al., 2020; Bi et al., 2021). Further investigation is warranted in this area. One of the limitations of our study is the use of a single hepatocyte lot. Nonetheless, transport data, particularly in plateable human hepatocytes, are consistent with our earlier reports across multiple hepatocyte lots for several OATP1B substrates evaluated here (pitavastatin, glyburide, montelukast, PF-05241328) (Bi et al., 2021). Finally,

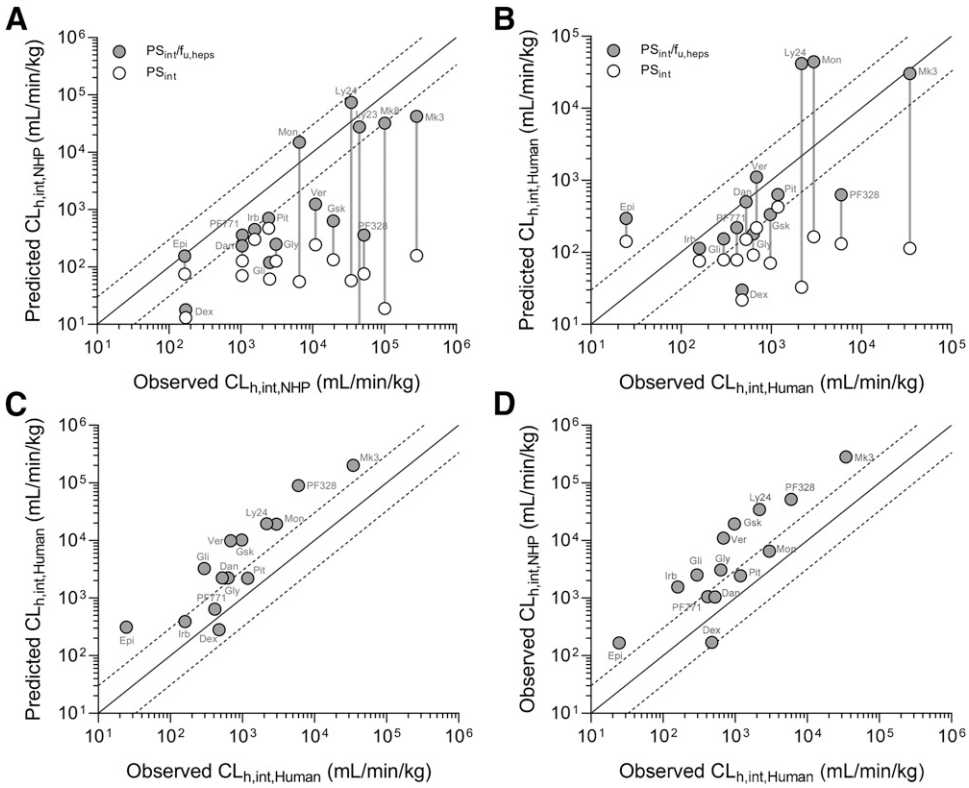

Fig. 4. In vitro–in vivo extrapolation to predict monkey and human hepatic intrinsic clearance based on hepatocyte uptake data. (A) Observed vs. predicted hepatic intrinsic clearance in NHP. (B) Observed vs. predicted hepatic intrinsic clearance in human. Predictions are based on direct scaling of uptake clearance measured in cultured monkey (A) or human (B) hepatocytes in the control condition (open points) and correcting for fraction unbound in the hepatocyte incubations (closed points). (C) Observed vs. predicted human hepatic intrinsic clearance, wherein predictions are based on scaling of uptake clearance measured in cultured human hepatocytes (Human PSinf/f$_{u,heps}$) corrected for compound-specific scaling factor (ratio of observed to predicted monkey clearance) obtained from IVIVE of monkey uptake clearance. (D) Observed human hepatic intrinsic clearance vs. observed monkey hepatic intrinsic clearance. Diagonal lines represent unity and ±3-fold error. Data points are labeled with compound code (see Table 1).

it is noteworthy that the measurement of nonspecific binding to cell systems at conditions used in the in vitro assays can be important in the translation of in vitro data. This is a common practice in the translation of in vitro metabolic clearance data obtained using liver microsomes or hepatocytes (Obach, 1997; Hallifax and Houston, 2012) and should be routinely considered in scaling transport clearance.

Earlier studies with extensive data sets suggested considerable underperformance in the translation of in vitro metabolic clearance measured using human liver microsomes or hepatocytes to

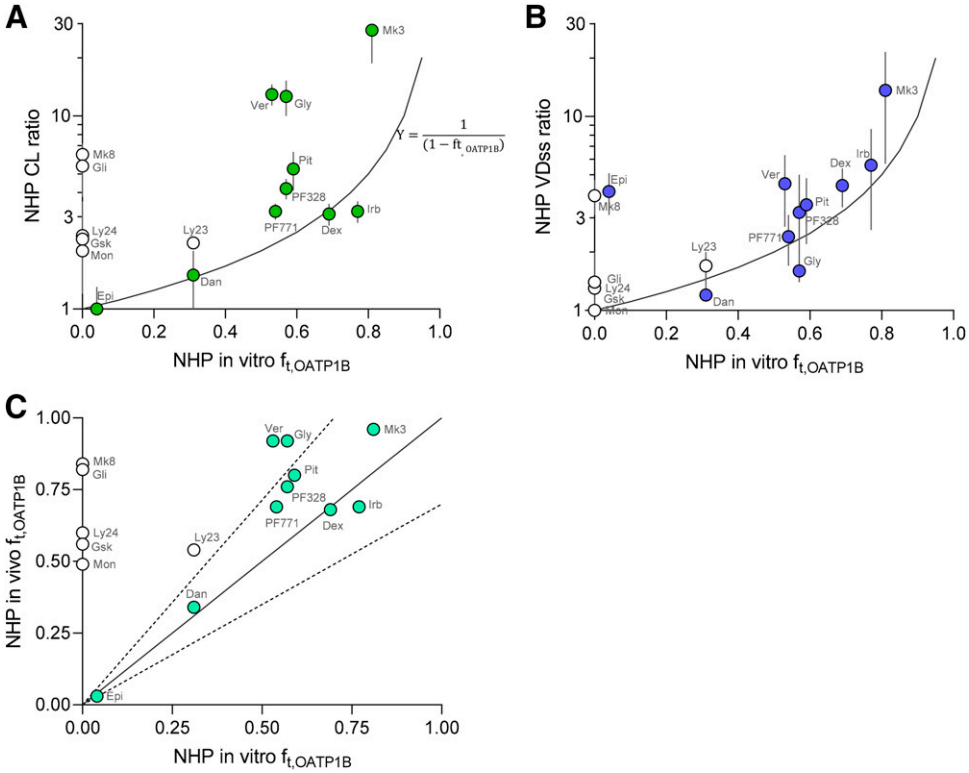

Fig. 5. Correlation between fraction transported by OATP1B in plated monkey hepatocytes and change in clearance (A) and change in VDss (B) in NHP after rifampicin treatment. Curves depict theoretical correlation (ratio = 1/(1−f$_{t,OATP1B}$)), assuming in vitro f$_{t,OATP1B}$ is equal to in vivo f$_{t,OATP1B}$, and rifampicin treatment completely abated OATP1B-mediated uptake in vivo. (C) In vitro vs. in vivo f$_{t,OATP1B}$. Solid and dashed lines represent unity ±30% error. Data points represent compounds with log P ≤6.5 (closed points) and log P >6.5 (open points). Data points show mean, and error bars when presented depict S.D. Data points are labeled with compound code (see Table 1).

predict human hepatic clearance for drugs thought to be cleared by metabolism alone (i.e., do not involve transporters) (Hallifax and Houston, 2012; Wood et al., 2017). However, it is well demonstrated that the fraction metabolism by a specific enzyme measured using these human reagents provides reliable quantitative predictions for the victim DDIs, particularly involving CYPs and UDP glucuronosyltransferases (Bjornsson et al., 2003; Di et al., 2013; https://wwwfdagov/regulatory-information/search-fda-guidance-documents/vitro-drug-interaction-studies-cytochrome-p450-enzyme-and-transporter-mediated-drug-interactions). Analogous to this, although we note considerable disconnect in the IVIVE of hepatic intrinsic clearance using in vitro PS_{inf} in both monkey and human, in vitro $f_{t,OATP1B}$ values obtained using hepatocytes are in good agreement with the in vivo change in clearance and VDss in the cynomolgus monkey after rifampicin administration (Fig. 5). Moreover, there is good concordance in the in vitro $f_{t,OATP1B}$ between monkey and human hepatocytes, reflecting on the likely translation of observed rifampicin-induced PK changes in cynomolgus monkey to human.

Conclusions

In conclusion, this study provides robust evidence for the important role of OATP1B1/1B3-mediated hepatic uptake in the clearance and VDss of large lipophilic acids (typically highly permeable and ECCS class 1B drugs/compounds). Although in vitro transporter data are helpful in many cases to quantify the uptake mechanism, certain limitations in the cell-based studies may result in considerable false negative readout. Consequently, further diligence using in vivo animal models, such as the cynomolgus monkey, becomes important to characterize hepatic uptake in this broader physicochemical space.

Acknowledgments

The authors wish to thank Brendan Tierney for supporting pharmacokinetic studies in cynomolgus monkeys. Keith Riccardi is acknowledged for conducting plasma protein binding measurements. John Curto is acknowledged for sourcing several of the study compounds. Robert Mongillo is acknowledged for providing analytical chemistry support. The authors also wish to thank David Edmonds, David Rodrigues, Theunis Goosen, Li Di, Dennis Scott, and Tristan Maurer for valuable input during this study.

Authorship Contributions

Participated in research design: Eng, Bi, Tess, Griffith, Litchfield, Kalgutkar, Varma.

Conducted experiments: Eng, Bi, West, Ryu, Yamaguchi, Kosa.

Performed data analysis: Eng, Bi, Tess, Varma.

Wrote or contributed to the writing of the manuscript: Eng, Bi, West, Ryu, Yamaguchi, Kosa, Tess, Griffith, Litchfield, Kalgutkar, Varma.

References

Alluri RV, Li R, and Varma MVS (2020) Transporter-enzyme interplay and the hepatic drug clearance: what have we learned so far? *Expert Opin Drug Metab Toxicol* **16**:387–401.

Bi YA, Costales C, Mathialagan S, West M, Eatemadpour S, Lazzaro S, Tylaska L, Scialis R, Zhang H, Umland J, et al. (2019) Quantitative contribution of six major transporters to the hepatic uptake of drugs: "SLC-phenotyping" using primary human hepatocytes. *J Pharmacol Exp Ther* **370**:72–83.

Bi YA, Ryu S, Tess DA, Rodrigues AD, and Varma MVS (2021) Effect of human plasma on hepatic uptake of organic anion-transporting polypeptide 1B substrates: studies using transfected cells and primary human hepatocytes. *Drug Metab Dispos* **49**:72–83.

Bi YA, Scialis RJ, Lazzaro S, Mathialagan S, Kimoto E, Keefer J, Zhang H, Vildhede AM, Costales C, Rodrigues AD, et al. (2017) Reliable rate measurements for active and passive hepatic uptake using plated human hepatocytes. *AAPS J* **19**: 787–796.

Bjornsson TD, Callaghan JT, Einolf HJ, Fischer V, Gan L, Grimm S, Kao J, King SP, Miwa G, Ni L, et al.; Pharmaceutical Research and Manufacturers of America (PhRMA) Drug Metabolism/Clinical Pharmacology Technical Working Group; FDA Center for Drug Evaluation and Research (CDER) (2003) The conduct of in vitro and in vivo drug-drug interaction studies: a Pharmaceutical Research and Manufacturers of America (PhRMA) perspective. *Drug Metab Dispos* **31**:815–832.

Bowman CM and Benet LZ (2018) An examination of protein binding and protein-facilitated uptake relating to in vitro-in vivo extrapolation. *Eur J Pharm Sci* **123**: 502–514.

Brennan BJ, Poirier A, Moreira S, Morcos PN, Goelzer P, Portmann R, Asthappan J, Funk C, and Smith PF (2015) Characterization of the transmembrane transport and absolute bioavailability of the HCV protease inhibitor danoprevir. *Clin Pharmacokinet* **54**:537–549.

Bteich M, Poulin P, and Haddad S (2019) The potential protein-mediated hepatic uptake: discussion on the molecular interactions between albumin and the hepatocyte cell surface and their implications for the in vitro-to-in vivo extrapolations of hepatic clearance of drugs. *Expert Opin Drug Metab Toxicol* **15**:633–658.

Chu X, Bleasby K, and Evers R (2013) Species differences in drug transporters and implications for translating preclinical findings to humans. *Expert Opin Drug Metab Toxicol* **9**:237–252.

Chu X, Shih SJ, Shaw R, Hentze H, Chan GH, Owens K, Wang S, Cai X, Newton D, Castro-Perez J, et al. (2015) Evaluation of cynomolgus monkeys for the identification of endogenous biomarkers for hepatic transporter inhibition and as a translatable model to predict pharmacokinetic interactions with statins in humans. *Drug Metab Dispos* **43**:851–863.

Davies B and Morris T (1993) Physiological parameters in laboratory animals and humans. *Pharm Res* **10**:1093–1095.

De Bruyn T, Ufuk A, Cantrill C, Kosa RE, Bi YA, Niosi M, Modi S, Rodrigues AD, Tremaine LM, Varma MVS, et al. (2018) Predicting human clearance of organic anion transporting polypeptide substrates using cynomolgus monkey: in vitro-in vivo scaling of hepatic uptake clearance. *Drug Metab Dispos* **46**: 989–1000.

Di L, Feng B, Goosen TC, Lai Y, Steyn SJ, Varma MV, and Obach RS (2013) A perspective on the prediction of drug pharmacokinetics and disposition in drug research and development. *Drug Metab Dispos* **41**:1975–1993.

Di L, Whitney-Pickett C, Umland JP, Zhang H, Zhang X, Gebhard DF, Lai Y, Federico JJ 3rd, Davidson RE, Smith R, et al. (2011) Development of a new permeability assay using low-efflux MDCKII cells. *J Pharm Sci* **100**:4974–4985.

Ebeling M, Küng E, See A, Broger C, Steiner G, Berrera M, Heckel T, Iniguez L, Albert T, Schmucki R, et al. (2011) Genome-based analysis of the nonhuman primate Macaca fascicularis as a model for drug safety assessment. *Genome Res* **21**: 1746–1756.

El-Kattan AF and Varma MVS (2018) Navigating transporter sciences in pharmacokinetics characterization using the extended clearance classification system. *Drug Metab Dispos* **46**:729–739.

Grover A and Benet LZ (2009) Effects of drug transporters on volume of distribution. *AAPS J* **11**:250–261.

Hallifax D and Houston JB (2012) Evaluation of hepatic clearance prediction using in vitro data: emphasis on fraction unbound in plasma and drug ionisation using a database of 107 drugs. *J Pharm Sci* **101**:2645–2652.

Higgins JW, Bao JQ, Ke AB, Manro JR, Fallon JK, Smith PC, and Zamek-Gliszczynski MJ (2014) Utility of Oatp1a/1b-knockout and OATP1B1/3-humanized mice in the study of OATP-mediated pharmacokinetics and tissue distribution: case studies with pravastatin, atorvastatin, simvastatin, and carboxydichlorofluorescein. *Drug Metab Dispos* **42**:182–192.

Hosea NA, Collard WT, Cole S, Maurer TS, Fang RX, Jones H, Kakar SM, Nakai Y, Smith BJ, Webster R, et al. (2009) Prediction of human pharmacokinetics from preclinical information: comparative accuracy of quantitative prediction approaches. *J Clin Pharmacol* **49**:513–533.

Iwasaki K and Uno Y (2009) Cynomolgus monkey CYPs: a comparison with human CYPs. *Xenobiotica* **39**:578–581.

Jiang Y, Andrews SW, Condroski KR, Buckman B, Serebryany V, Wenglowsky S, Kennedy AL, Madduru MR, Wang B, Lyon M, et al. (2014) Discovery of danoprevir (ITMN-191/R7227), a highly selective and potent inhibitor of hepatitis C virus (HCV) NS3/4A protease. *J Med Chem* **57**:1753–1769.

Jones HM, Barton HA, Lai Y, Bi YA, Kimoto E, Kempshall S, Tate SC, El-Kattan A, Houston JB, Galetin A, et al. (2012) Mechanistic pharmacokinetic modeling for the prediction of transporter-mediated disposition in humans from sandwich culture human hepatocyte data. *Drug Metab Dispos* **40**:1007–1017.

Kim SJ, Lee KR, Miyauchi S, and Sugiyama Y (2019) Extrapolation of in vivo hepatic clearance from in vitro uptake clearance by suspended human hepatocytes for anionic drugs with high binding to human albumin: improvement of in vitro-to-in vivo extrapolation by considering the "albumin-mediated" hepatic uptake mechanism on the basis of the "facilitated-dissociation model". *Drug Metab Dispos* **47**: 94–103.

Kimoto E, Bi YA, Kosa RE, Tremaine LM, and Varma MVS (2017) Hepatobiliary clearance prediction: species scaling from monkey, dog, and rat, and In Vitro-In Vivo extrapolation of sandwich-cultured human hepatocytes using 17 drugs. *J Pharm Sci* **106**:2795–2804.

Kosa RE, Lazzaro S, Bi YA, Tierney B, Gates D, Modi S, Costales C, Rodrigues AD, Tremaine LM, and Varma MV (2018) Simultaneous assessment of transporter-mediated drug-drug interactions using a probe drug cocktail in cynomolgus monkey. *Drug Metab Dispos* **46**:1179–1189.

Liang X, Park Y, DeForest N, Hao J, Zhao X, Niu C, Wang K, Smith B, and Lai Y (2020) In vitro hepatic uptake in human and monkey hepatocytes in the presence and absence of serum protein and its in vitro to in vivo extrapolation. *Drug Metab Dispos* **48**:1283–1292.

Liao M, Zhu Q, Zhu A, Gemski C, Ma B, Guan E, Li AP, Xiao G, and Xia CQ (2019) Comparison of uptake transporter functions in hepatocytes in different species to determine the optimal model for evaluating drug transporter activities in humans. *Xenobiotica* **49**:852–862.

Ménochet K, Kenworthy KE, Houston JB, and Galetin A (2012) Use of mechanistic modeling to assess interindividual variability and interspecies differences in active uptake in human and rat hepatocytes. *Drug Metab Dispos* **40**:1744–1756.

Miyauchi S, Masuda M, Kim SJ, Tanaka Y, Lee KR, Iwakado S, Nemoto M, Sasaki S, Shimono K, Tanaka Y, et al. (2018) The phenomenon of albumin-mediated hepatic uptake of organic anion transport polypeptide substrates: prediction of the in vivo uptake clearance from the in vitro uptake by isolated hepatocytes using a facilitated-dissociation model. *Drug Metab Dispos* **46**:259–267.

Obach RS (1997) Nonspecific binding to microsomes: impact on scale-up of in vitro intrinsic clearance to hepatic clearance as assessed through examination of warfarin, imipramine, and propranolol. *Drug Metab Dispos* **25**:1359–1369.

Press B and Di Grandi D (2008) Permeability for intestinal absorption: caco-2 assay and related issues. *Curr Drug Metab* **9**:893–900.

Prueksaritanont T, Chu X, Evers R, Klopfer SO, Caro L, Kothare PA, Dempsey C, Rasmussen S, Houle R, Chan G, et al. (2014) Pitavastatin is a more sensitive and selective organic anion-transporting polypeptide 1B clinical probe than rosuvastatin. *Br J Clin Pharmacol* **78**:587–598.

Riccardi K, Ryu S, Lin J, Yates P, Tess D, Li R, Singh D, Holder BR, Kapinos B, Chang G, et al. (2018) Comparison of species and cell-type differences in fraction unbound of liver tissues, hepatocytes, and cell lines. *Drug Metab Dispos* **46**:415–421.

Riccardi KA, Tess DA, Lin J, Patel R, Ryu S, Atkinson K, Di L, and Li R (2019) A novel unified approach to predict human hepatic clearance for both enzyme- and transporter-mediated mechanisms using suspended human hepatocytes. *Drug Metab Dispos* **47**:484–492.

Rodgers T and Rowland M (2007) Mechanistic approaches to volume of distribution predictions: understanding the processes. *Pharm Res* **24**:918–933.

Ryu S, Tess D, Chang G, Keefer C, Burchett W, Steeno GS, Novak JJ, Patel R, Atkinson K, Riccardi K, et al. (2020) Evaluation of fraction unbound across 7 tissues of 5 species. *J Pharm Sci* **109**:1178–1190.

Salphati L, Chu X, Chen L, Prasad B, Dallas S, Evers R, Mamaril-Fishman D, Geier EG, Kehler J, Kunta J, et al. (2014) Evaluation of organic anion transporting polypeptide 1B1 and 1B3 humanized mice as a translational model to study the pharmacokinetics of statins. *Drug Metab Dispos* **42**:1301–1313.

Shalaeva M, Kenseth J, Lombardo F, and Bastin A (2008) Measurement of dissociation constants (pKa values) of organic compounds by multiplexed capillary electrophoresis using aqueous and cosolvent buffers. *J Pharm Sci* **97**:2581–2606.

Shen H, Dai J, Liu T, Cheng Y, Chen W, Freeden C, Zhang Y, Humphreys WG, Marathe P, and Lai Y (2016) Coproporphyrins I and III as functional markers of OATP1B activity: in vitro and in vivo evaluation in preclinical species. *J Pharmacol Exp Ther* **357**:382–393.

Shen H, Su H, Liu T, Yao M, Mintier G, Li L, Fancher RM, Iyer R, Marathe P, Lai Y, et al. (2015) Evaluation of rosuvastatin as an organic anion transporting polypeptide (OATP) probe substrate: in vitro transport and in vivo disposition in cynomolgus monkeys. *J Pharmacol Exp Ther* **353**:380–391.

Shen H, Yang Z, Mintier G, Han YH, Chen C, Balimane P, Jemal M, Zhao W, Zhang R, Kallipatti S, et al. (2013) Cynomolgus monkey as a potential model to assess drug interactions involving hepatic organic anion transporting polypeptides: in vitro, in vivo, and in vitro-to-in vivo extrapolation. *J Pharmacol Exp Ther* **344**: 673–685.

Smith DA, Beaumont K, Maurer TS, and Di L (2015) Volume of distribution in drug design. *J Med Chem* **58**:5691–5698.

Steyn SJ and Varma MVS (2020) Cytochrome-P450-mediated drug-drug interactions of substrate drugs: assessing clinical risk based on molecular properties and an extended clearance classification system. *Mol Pharm* **17**:3024–3032.

Stopher D and McClean S (1990) An improved method for the determination of distribution coefficients. *J Pharm Pharmacol* **42**:144.

Takahashi T, Ohtsuka T, Yoshikawa T, Tatekawa I, Uno Y, Utoh M, Yamazaki H, and Kume T (2013) Pitavastatin as an in vivo probe for studying hepatic organic anion transporting polypeptide-mediated drug-drug interactions in cynomolgus monkeys. *Drug Metab Dispos* **41**:1875–1882.

Tess DA, Eng H, Kalgutkar AS, Litchfield J, Edmonds DJ, Griffith DA, and Varma MVS (2020) Predicting the human hepatic clearance of acidic and zwitterionic drugs. *J Med Chem* **63**:11831–11844.

Thakare R, Gao H, Kosa RE, Bi YA, Varma MVS, Cerny MA, Sharma R, Kuhn M, Huang B, Liu Y, et al. (2017) Leveraging of rifampicin-dosed cynomolgus monkeys to identify bile acid 3-O-sulfate conjugates as potential novel biomarkers for organic anion-transporting polypeptides. *Drug Metab Dispos* **45**:721–733.

Ufuk A, Kosa RE, Gao H, Bi YA, Modi S, Gates D, Rodrigues AD, Tremaine LM, Varma MVS, Houston JB, et al. (2018) In vitro-in vivo extrapolation of OATP1B-mediated drug-drug interactions in cynomolgus monkey. *J Pharmacol Exp Ther* **365**:688–699.

Varma MV, Bi YA, Kimoto E, and Lin J (2014) Quantitative prediction of transporter- and enzyme-mediated clinical drug-drug interactions of organic anion-transporting polypeptide 1B1 substrates using a mechanistic net-effect model. *J Pharmacol Exp Ther* **351**:214–223.

Varma MV, El-Kattan AF, Feng B, Steyn SJ, Maurer TS, Scott DO, Rodrigues AD, and Tremaine LM (2017a) Extended Clearance Classification System (ECCS) informed approach for evaluating investigational drugs as substrates of drug transporters. *Clin Pharmacol Ther* **102**:33–36.

Varma MV, Gardner I, Steyn SJ, Nkansah P, Rotter CJ, Whitney-Pickett C, Zhang H, Di L, Cram M, Fenner KS, et al. (2012) pH-Dependent solubility and permeability criteria for provisional biopharmaceutics classification (BCS and BDDCS) in early drug discovery. *Mol Pharm* **9**:1199–1212.

Varma MV, Kimoto E, Scialis R, Bi Y, Lin J, Eng H, Kalgutkar AS, El-Kattan AF, Rodrigues AD, and Tremaine LM (2017b) Transporter-mediated hepatic uptake plays an important role in the pharmacokinetics and drug-drug interactions of montelukast. *Clin Pharmacol Ther* **101**:406–415.

Varma MV, Steyn SJ, Allerton C, and El-Kattan AF (2015) Predicting clearance mechanism in drug discovery: extended clearance classification system (ECCS). *Pharm Res* **32**:3785–3802.

Watanabe T, Kusuhara H, Maeda K, Shitara Y, and Sugiyama Y (2009) Physiologically based pharmacokinetic modeling to predict transporter-mediated clearance and distribution of pravastatin in humans. *J Pharmacol Exp Ther* **328**:652–662.

Wood FL, Houston JB, and Hallifax D (2017) Clearance prediction methodology needs fundamental improvement: trends common to rat and human hepatocytes/microsomes and implications for experimental methodology. *Drug Metab Dispos* **45**:1178–1188.

Zheng HX, Huang Y, Frassetto LA, and Benet LZ (2009) Elucidating rifampin's inducing and inhibiting effects on glyburide pharmacokinetics and blood glucose in healthy volunteers: unmasking the differential effects of enzyme induction and transporter inhibition for a drug and its primary metabolite. *Clin Pharmacol Ther* **85**:78–85.

Address correspondence to: Manthena V. S. Varma, ADME Sciences, Medicine Design, Worldwide Research and Development, MS 8220-2451, Pfizer Inc., Groton, CT 06340. E-mail: manthena.v.varma@pfizer.com